



Optical detection of ammonia inside a stack: Comparison of different techniques



F. D'Amato^{a,*}, S. Viciani^a, A. Montori^a, A. Lapini^{a,1}, I. Fraboulet^b, J. Poulleau^b

^a CNR-INO, Largo E. Fermi 6, 50125 Firenze, Italy

^b INERIS, Parc technologique Alata, BP 2, 60550 Verneuil-en-Halatte, France

ARTICLE INFO

Article history:

Received 31 October 2019

Received in revised form 20 January 2020

Accepted 11 March 2020

Available online 18 March 2020

Keywords:

Biomass burning

Calibration issues

Ammonia

Optical detection techniques

Multipass cell

Stack measurements

ABSTRACT

The quantitative detection of pollutants in industrial emissions, in particular the emissions of biomass burners, requires different types of analyzers. Optical devices are usually sensitive to the transparency and dirtiness of the exhaust gases, so optical measurements are normally carried out by extracting the samples from the stacks. This paper has a twofold aim. First, we will prove that the molecular composition of the exhaust mixture (in particular the concentration of water and carbon dioxide) can deeply affect the outcome of optical analyzers, depending on the adopted detection technique. This is a critical issue, in particular with a view to the necessity of providing suitable reference methods for monitoring biomass burners emissions. Second, we will show how it is possible to measure inside an artificial stack by using an optical multipass cell located across the gas flow, even at 140 °C, or in presence of soot.

© 2020 The Authors. Published by Elsevier Ltd. This is an open access article under the CC BY-NC-ND license (<http://creativecommons.org/licenses/by-nc-nd/4.0/>).

1. Introduction

Combustion of biomass is gaining an increasing attention as a renewable energy source, alternative to fossil fuels. Despite the common popular feeling which considers biomass burners as eco-friendly, their emissions contain several substances to be strictly monitored and limited: besides water and carbon dioxide, the exhaust gases also include [1] CO, NO_x, CH₄, NH₃, Volatile Organic Compounds (VOCs), HCl, SO₂, and a significant content of fine dust. In general, measuring the composition of the exhaust gases in an industrial combustion process is very important for two reasons: it provides information about the process itself, so allowing a feedback towards the process parameters (for instance fuel/oxygen ratio), in order to optimize it [2,3]. Moreover, it allows monitoring the amount of pollutants released by the plant, which should be kept within the limits set by regulations. While thermo-electric plants and incinerators are already regulated by national and international laws, some Standard Reference Methods (SRMs) are still incomplete or missing for pollutant concentrations in biomass burning plants (e.g. for remote domestic heating) and in general for flow velocity in narrow ducts (typical of biomass burners). Project EMPIR-EURAMET IMPRESS-2, Metrology for Air Pollutant

Emissions (<http://empir.npl.co.uk/impress/>) has among its tasks the analysis of the possible interferences by foreign gases, in the spectroscopical measurements of ammonia and hydrogen chloride, for biomass burners. The activity described in this paper aims to the assessment of the effects of gas composition in a stack simulator, on the measurements of ammonia with two different techniques, namely Direct Absorption (DA) and Wavelength Modulation Spectroscopy (WMS). The aim of this research is not to validate one or both techniques according to EN 15267-3 or 14793, as some commercial analyzers already passed this test (for instance LaserGas II SP by NEO Monitors AS and LD6 by Siemens AG). The aim is to verify if special experimental conditions can affect calibration. For this purpose we realized a gas analyzer whose electronic core is a general purpose one, suitable to be used with several different gases, while the optical setup was tailored on the specific application and experimental conditions. In particular, to our knowledge this is the first description of a multipass cell inserted inside a stack. By the way, our solution doesn't need heated pipes and measurement cells, to avoid the condensation of the usually high water concentration, outside the stack. This optical device will be described in details. We experienced no problems of stability or mirrors cleanliness when ammonia was added in the stack to the exhausts of a methane burner, while mirrors suffered contamination when burning gasoline or wooden pellets because of soot or ashes. Anyway, we have a ready solution

* Corresponding author.

E-mail address: francesco.damato@cnr.it (F. D'Amato).

URL: <https://fox.ino.it/home/damato/> (F. D'Amato).

¹ Present address: INRIM, Strada delle Cacce 91, 10135 Torino, Italy.

for such cases, in order to allow long-lasting measurements also in case of dirty exhausts.

2. Calibration issues for optical techniques

Let's examine in details the impact of mixture composition on spectroscopic detection techniques. Several techniques and commercial devices are commonly used to measure the content of different molecules in the exhausts of combustors, directly inside the burners or stacks, or with the extraction of gases, to be analyzed immediately outside, or with a complete off-line measurement. Many analyzers rely on optical techniques, both inside and outside the stacks. Optical diffusion and scattering are worldwide used to measure concentration and size of dust particles [4]. As for the concentration of gaseous chemicals, applied spectroscopy is being used since about three decades for the quantitative detection of the most common species in industrial emission: carbon monoxide and dioxide, hydrogen chloride and fluoride, ammonia, and several more.

Several techniques have been proposed for this application: DA; low-frequency modulation spectroscopy WMS [5]; high-frequency modulation spectroscopy (the so-called FMS [6,7]); two-tone frequency modulation spectroscopy (TTFM [8,9]); photo-acoustic spectroscopy (PAS [10]) and its recent development, Quartz-Enhanced Photo Acoustic Spectroscopy (QEPAS [11,12]); cavity ring-down-spectroscopy (CRDS [13]).

All these techniques are based on the Beer-Lambert law:

$$I_{out} = I_{in} \cdot e^{-\alpha L} \quad (1)$$

where I_{out} and I_{in} are the powers of the light beam after and before crossing the sample, respectively; L is the length of the sample, and

$$\alpha = S \cdot g(\nu) \cdot n \quad (2)$$

where S (cm/molecule) is the absorption strength, $g(\nu)$ (cm) the shape of the absorption (area normalized to 1), and n (molecule/cm³) the density of the absorbing species.

Of course, each technique has advantages and drawbacks, and different operational constraints. For instance, PAS and QEPAS work better at pressures below atmospheric pressure [14,15], CRDS requires samples without dust, as dust could reduce the reflectivity of the mirrors [16], FMS is simpler with narrow absorption profiles [6], and so on. As a matter of fact, the simplest and most robust techniques, despite their being the most affected by noise, are DA and WMS. They don't require high frequency circuitry, low pressures, clean samples. WMS exhibits a better signal-to-noise with respect to DA, while maintaining a simple implementation, and for this reason is mostly used in commercial devices [17]. Yet, some precautions must be adopted. When temperature, pressure or mixture composition change, there is a variation of the shape of the absorption profile too. In Ref. [18] it's shown how the same concentration of methane, at different pressures, requires different approaches for a correct derivative detection, as the shape of the absorption profile significantly changes. Similar effects can be obtained by changing the composition of the mixture, as each gas has its own broadening effect when colliding against other molecules. This problem can be easily managed by DA [19]. The most effective way of retrieving the concentration is to measure the integral of the absorbance. This value only depends on the density of absorbers, whatever the lineshape:

$$n = \frac{\int_{-\infty}^{+\infty} -\ln \frac{I_{out}}{I_{in}} d\nu}{L \cdot S(T)} \quad (3)$$

So, provided that the laser scan is large enough, with respect to the absorption linewidth, this integral can always be calculated unambiguously. Anyway, the wide laser scan is only necessary to acquire

as many datapoints as possible, because we first fit the absorption with a theoretical function including all the involved transitions, and then integrate line by line the fitted profile. In this way we can obtain reliable results also in case of overlapping absorptions. As for WMS, when the detection is at $2f$ (with f modulation frequency), the density of absorbers is proportional to the height of the central peak (or to the difference between the central and the side peaks). But this peak flattens with increasing absorption linewidth due to increasing pressure or, for instance, to the presence of foreign perturbers, like water or carbon dioxide. In practice, when in a sample the density of the target molecule is constant, the height of the central peak depends on temperature, or on the varying densities of other gases. Modeling this effect on WMS is a complex task, especially in stand-alone, unattended devices, as several parameters are involved, like the coupling of the frequency modulation into the laser, the modulation depth, the effectiveness of the retrieval algorithm in correcting for lineshape. For instance, a change in the laser operating point, due to ageing or sensitivity to the external temperature, would require a different set of fit parameters. A solution for some of these drawbacks is the normalization of the second derivative value to the first derivative [20,21]. As both signals feature the same dependence on laser power, modulation width and depth and, to a great extent, absorption lineshape, this normalization strongly reduces the sensitivity of the system to variations of the experimental parameters. Yet, this normalization does not cancel all the uncertainties, and the dependence of the signal baselines on the laser settings is a feature that can still yield problems.

When WMS is used to monitor industrial plants, some experimental conditions are more favorable than other ones. A thermo-electric plant burning fossil coal has a limited range of variation of the composition of the exhaust gases [22], and the content of water in the exhaust is negligible. An incinerator plant suffers the inhomogeneity of garbage. When biomass is burnt the density of the fuel, and the content of water in the material introduced into the burner, can significantly affect the content of carbon dioxide and water in the exhaust. These two molecules, among those commonly found in exhaust gases, are the most effective in changing width (and position) of absorption lines in general, and in particular of ammonia [23]. Moreover, the diameters of the stacks of biomass burners are typically narrower (~ 0.5 m) than those of incinerators. This makes no difference for analyzers which measure extracted samples, but can make a difference for optical, across-stack measurements. Due to the characteristics described above, it's necessary to verify the proper behavior of techniques and devices, already used in different applications, once moved to monitor biomass burners exhausts.

3. Experimental setup

The measurements were carried out at the INERIS facility in Verneuil-en-Halatte. The artificial stack is a 15 cm (internal diameter) titanium pipe with three different burners, one injection point for adding other gases to the exhaust flow, twelve ports for instrumentation, and exhaust. The mixture inside is almost totally recirculated. It's equipped with several controlling instruments, in order to allow a continuous check of the operating conditions. A Fourier transform gas analyser (Gasetm DX4000) is used to control the concentrations of the constituents of the mixture, and to provide a feedback to the injectors of sticky and reactive molecules (e.g. ammonia). In the artificial stack at INERIS it is possible to create a gas mixture, containing the target molecule at known mixing ratio, whose temperature (140 °C for the reported measurements) is maintained by combustion (of methane, diesel fuel, or wood pellets), or by electric heating. The difference in the two cases is that when heating is obtained by combustion, the mixture contains CO₂

and water at mixing ratios around 7–16%; with electric heating we have just hot air (CO₂ 500 ppm, water 1.5%) as the carrier gas.

While the electronics of our analyzer is a general-purpose one, the optics was tailored on the stack parameters. Let's examine in detail the different parts of our device.

3.1. Electronics

A block diagram of the electronics is shown in Fig. 1. A DFB laser (Norcada NL1512-B, wavelength 1512 nm, butterfly package, pigtail output) is supplied and stabilized in temperature by an integrated current supply/temperature stabilizer (ppqSense QubeCL). A National Instruments crate (cRIO 9067) hosts: a 4-channels, 20 MSamples/s acquisition rate each, 14 bits vertical resolution ADC plug-in (NI-9775); a programmable, 4-channels digital I/O plug-in (NI-9402); and a 4-channels PT100 reader (NI-9217). The cRIO crate has 8 slots for plug-ins, and other versions exist, with 4 slots, which in principle could have been used. But the selected version featured the most powerful CPU, and the widest operating temperature range of the series. A Tektronix double output Arbitrary Function Generator 3022 provided the low frequency (~ 1 kHz) sawtooth ramp to sweep the laser frequency across an absorption profile, and the high frequency (1 MHz) sinusoid used for the derivative detection. Both signals were sent to the QubeCL, to be converted in current and added to the bias current of the laser. A very important feature for the proper working of the system is the timing among the different signals. In order to set a common time reference we modified the NI-9775 plug-in, adding a test point where the 20 MHz clock is available. This TTL signal is sent to a home made divider, which provides a 10 MHz clock to the Tektronix function generator (which doesn't accept input frequencies

higher than 15 MHz). The latter device issues a trigger linked to the 1 kHz sawtooth ramp. This trigger is detected by the Digital I/O plug-in, and this event starts the acquisition. This means that the acquisition, and all the data treatments for derivative detection, are driven by the same clock, and maintain the relative phases. A diagram of the signal timing is shown in Fig. 2. The detectors are Hamamatsu InGaAs mod. G12180-210A, 1 mm diameter, 2-stage Peltier cooling, 40 MHz cutoff frequency. The preamplifiers of the detectors are home made. The circuitry connected to the reference detector amplifies the signal as-it-is. The main detector preamplifier provides an unfiltered output for direct absorption, and a high pass output for derivative detection (cutoff at 100 kHz).

We need to acquire pressure and temperature of the gas. For the measurement of pressure we selected a sensor by Honeywell, model SRNN1.6BA7A3, which is read by the QubeCL. This sensor is temperature compensated in the range $-20/+85$ °C, accuracy $\pm 0.25\%$ of the full scale, resolution 14 bit, reading I²C. Of course, it's not possible to insert this sensor inside the stack. So we connected the sensor, located close to the QubeCL, to the stack by means of a PTFE pipe, so allowing room temperature operation. The temperature sensor is a PT100, read by the specific NI plug-in.

3.2. Mechanics

The mechanics is divided into two parts. The first one hosts the electronics, the laser and the reference optics (Fig. 3, see Section 3.3). It is composed by an aluminum plate, reinforced by aluminum profiles, forming a frame which fits the interior of a plastic case suitable for shipping. All the devices are firmly tightened to the plate or to the profiles, including cables and a power strip.

The other part of the mechanics is mounted onto the stack (Fig. 4). An aluminum plate fits the aperture in the stack. It hosts two Swagelok ports, one to insert the PT100 across the gas flow, the other one to connect the PTFE pipe for the reading of the pressure. A central hole allows the insertion of the multipass cell (see Section 3.3). We had to take care of the thermal effects on launching and receiving optics. So, the circular plate holding all the optics, and the holder of the fiber collimator and the detector, are made of stainless steel, which features a lower thermal conduction coefficient than aluminum (16 against 205 W/m·K, respectively). Moreover, between the holding disk and the two holders of the detector and the launching optics there is a 2-mm thick layer of MACOR[®] (1.46 W/mK). A thick layer of silicon rubber is inserted between the stainless steel disk and the aluminum plate, to further reduce the heat transmission towards the exterior. Finally, a metallic box, containing the preamplifier of the main detector, is fixed onto this plate.

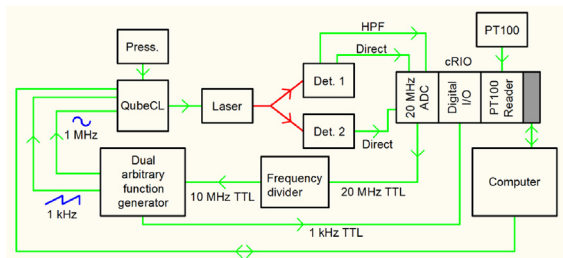


Fig. 1. Block diagram of the electronics. HPF: High Pass Filter.

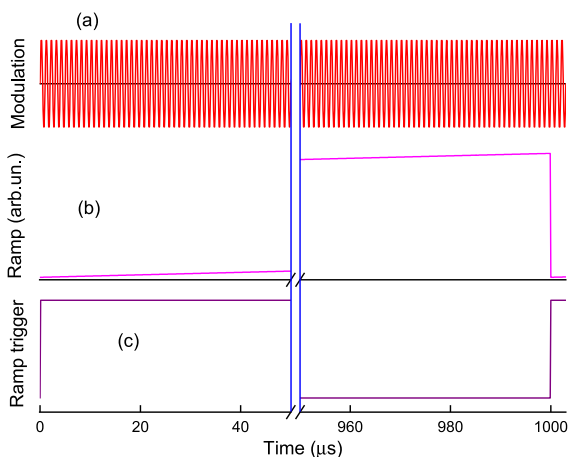


Fig. 2. Timing of the different signals: (a) Modulation at 1 MHz applied to the laser. (b) Current ramp at 1 kHz applied to the laser. (c) Trigger for the current ramp. All signals maintain the relative phases among themselves.

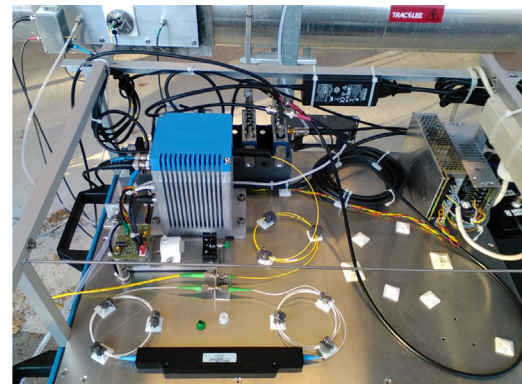


Fig. 3. Photo of the main plate of the mechanics.

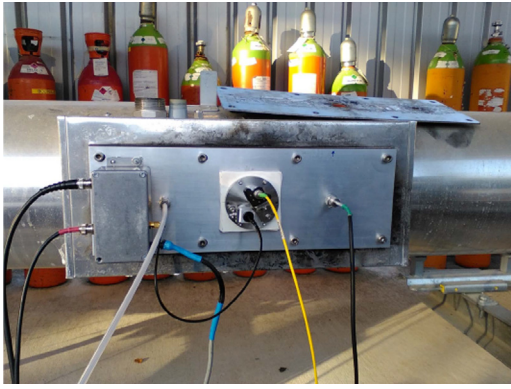


Fig. 4. Photo of the parts installed on the stack. The preamplifier is inside the metallic box on the left.

3.3. Optics

As the laser is fiber-coupled, most of the optical path outside the stack occurs through fibers (Fig. 5). The laser light can be directly sent to the measurement cell, or to a BK7 etalon (Free Spectral Range (FSR) 0.1083 cm^{-1}), directly or after crossing a reference cell (Wavelength References NH3-100, fiber coupled, 100 mBar NH_3 , 16.5 cm optical path). The measurement cell is a home-made Herriott cell, with a distance of 199 mm between the mirrors, and 48 passes, providing a total pathlength of 9.70 m, including the path behind the In/Out mirror. The material of the mirrors is fused silica, and the spacers are six carbon fibers pipes (5 mm external diameter, 4 mm internal diameter). These pipes are arranged in the standard configuration which constrains

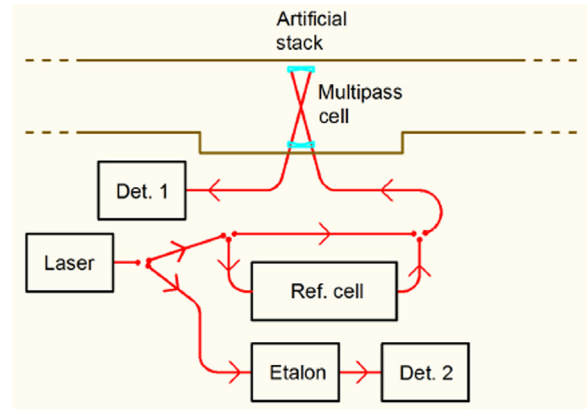


Fig. 5. Block diagram of the optics.

the possible degrees of freedom (Figs. 4, 6). The mirrors are glued inside an aluminum holder, which in turn is glued to the spacers. The glue is Masterbond EP21TCHT-1, with operating temperature range $4 \text{ K} \div 204 \text{ }^\circ\text{C}$. The spots arrangement onto the mirrors can be seen in Fig. 6 Left. The foreground mirror is seen from its back side, yet the red spots are visible, as its coating is not metallic, but dielectric, with reflectivity 97% at 635 nm and more than 99% at 1510 nm. The red light crossing the mirror is due to the remaining 3%. It is evident that one red spot is missing. This is because the standard arrangement of a Herriott cell is with entrance and exit across the same hole. But here we renounced to the last two passes inside the cell, in order to separate the beams outside the cell. This is explained in Fig. 6 Right. The green beam is the entrance beam, the blue beam is the actual exit beam. Without the existing exit

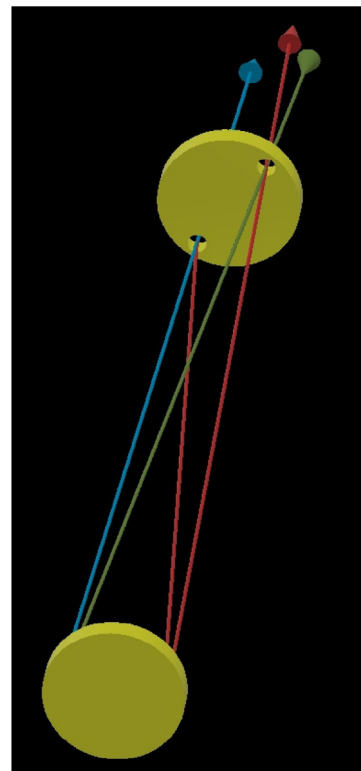
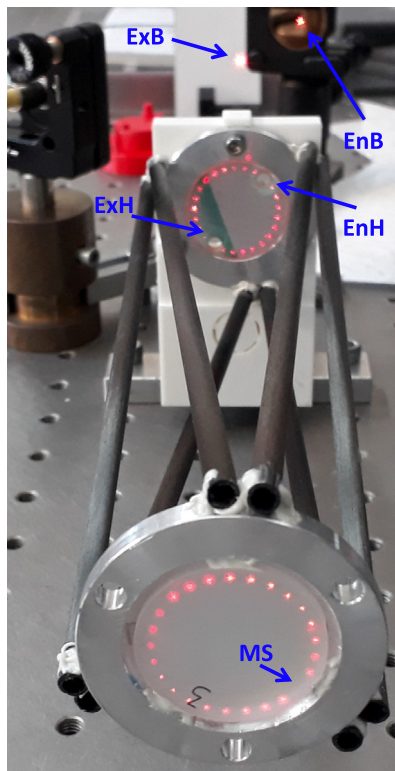


Fig. 6. Left: Photo of the multipass cell with a red beam showing the spots: (ExB) Exit beam; (EnB) Entrance Beam; (EnH) Entrance Hole; (ExH) Exit Hole; (MS) Missing Spot. Right: CAD rendering of the entrance (green), exit (blue), and missing (red) beams. (For interpretation of the references to colour in this figure legend, the reader is referred to the web version of this article.)

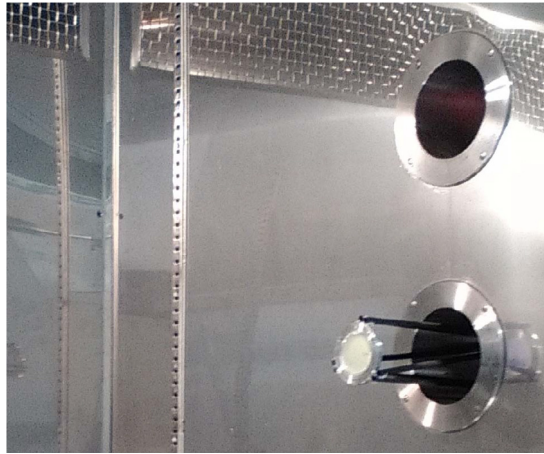


Fig. 7. Photo of the multipass cell inside the climatic chamber for the test of temperature stability.

hole, the beam would have been reflected two more times, and then would have left the cell across the entrance hole. The red beams describe this case, which is the standard for Herriott cells. All the other beams were omitted, for the sake of clarity. This makes the optomechanics outside the stack much easier and compact. The entrance and exit holes on the background mirror are clearly visible in Fig. 6 Left. Before the campaign we tested the stability of the cell in our climatic chamber at 100 °C (Fig. 7).

The apertures in the steel disk are sealed by two anti-reflection coated BK7 windows (Thorlabs WG10530-C), one for each beam.

3.4. Software

This analyzer is not a commercial instrument, but is intended for research applications, so it's not necessary to have a software which drives all the components automatically. Moreover, the electronics of the analyzer is based on three different stand-alone devices, namely the National Instrument system, the QubeCL and the Tektronix function generator. So we manually operated the function generator, we used the firmware of the QubeCL to set the laser and to control the modulations, and we wrote a LabVIEW program to drive the NI cRIO and realize the digital lock-in amplifier. The latter application is a well known one [24–26], so we'll describe in the following only the details related to our own implementation. The signals acquired in direct mode are just averaged using the FPGA of the cRIO, and the final waveforms are stored for later analysis.

We plan to use this electronic and software core for different applications. For the purposes of the present work we needed to scan the laser wavelength across an absorption profile, using direct absorption and second derivative for the retrieval of concentrations, and optionally first derivative for normalization.

In order to set the modulation frequency two opposite requirements must be taken into account. The laser $1/f$ noise “knee” is within 1 MHz [27]. At demodulation frequencies above this value the contribution of this noise to the overall noise will be negligible. The upper limit to the modulation frequency is imposed by the acquisition rate of the ADC which, in our case, is 20 MS/s simultaneously for its four channels. This means that when a modulation frequency of 1 MHz is applied, 20 points per modulation cycle will be acquired. For $2f$ demodulation, we have 10 points for each demodulation cycle. Further reduction of the number of points per demodulation period would compromise our signal to noise ratio, therefore the modulation frequency was then settled to 1 MHz.

The bottleneck of the data transmission chain is that the ADC can forward the acquired data to the FPGA of the cRIO at 4 MS/s. We decided to acquire 20 kS and then to transmit the data for further treatment. During data transmission the laser scan and the 1 MHz modulation were not interrupted, in order to keep the laser setpoint as stable as possible.

The sets of 20 kS, at the ramp frequency of 1 KHz (1000 ramps per second), acquired at 20 MS/s, correspond to a laser ramp scan. To obtain the first and second derivative curves, the demodulation was performed using a block multiplication scheme. Namely, each ramp has been divided in 200 blocks, each block containing 100 pts. Each point of the first and second derivative was hence obtained by multiplying 100 points of modulation times 100 points of the demodulating function (5 cycles for f and 10 cycles for $2f$ demodulation) and then summing them up. The block multiplication scheme was performed within the NI-Crio FPGA using two pre-defined 100 points sinusoidal lookup tables, set at f and $2f$ frequencies, respectively.

3.5. Measurements

The measurements were carried out in five days, from October 15 to October 19, 2018, at the premises of INERIS, at Verneuil-en-Halatte (F). Our measurements at INERIS followed almost completely a scheduled test on the stack. This test aimed to validate the Gaset DX 4000 against the reference NF X 43-303, according to EN 14793. For a few extra measurements, the experimental conditions were changed on purpose. The tests lasted five days. Day 1 was used for installation. During days 2 and 3 an increasing concentration of ammonia, from values around 1 ppm to 26 ppm, was added to the exhaust of methane combustion. In day 4 diesel fuel was burned (ammonia concentration in the range 28–51 ppm), while in day 5 the fuel was wooden pellets (ammonia concentration in the range 7–50 ppm). Temperature of the gas always was 140 °C, and the concentration of H₂O and CO₂ was due to the combustion. At the end of days 3 and 4, three measurements were carried out with the same temperature, but heating the air electrically, without any combustion. The optical behavior of the multipass cell, with the methane burner on, is shown in Fig. 8, where the direct absorption signal at 51 ppm ammonia mixing ratio and its fit are shown in the upper side, while the residual (magnified by a factor of 10^4) is shown at the bottom. The RMS of the residual is 10^{-4} , which includes optical fringes and any other noise. Changes of temperature can affect the alignment, and this could cause a reduction of output power. The fringe level depends

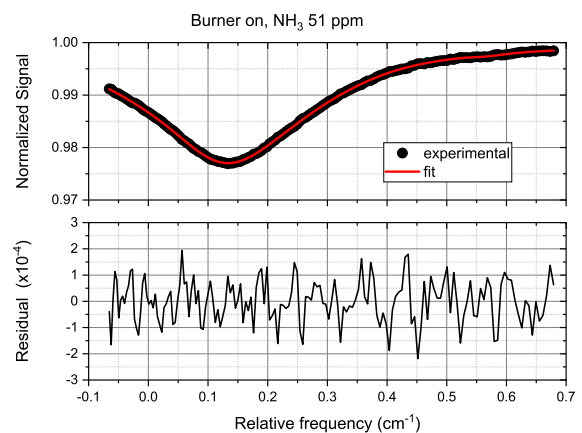


Fig. 8. Absorption signal and related fit, with the methane burner on, at an ammonia mixing ratio of 51 ppm (top), and residual, magnified by a factor of 10^4 (bottom).

on the possibility, for a fraction of the light, to be trapped as a stationary wave between two surfaces along the optical path. This can be caused by the geometry of the optical system, or by dirtiness on the mirrors of the multipass cell. Temperature cannot affect these two features, and so fringe level does not depend on temperature. We verified that the transmission of the optics inside the stack was constant during the days in which methane was used as a fuel, decreased with diesel fuel, and decreased even more with wooden pellets, when the presence of soot was well evident. Anyway, it is possible to protect the mirrors from soot or other contaminants, simply by using air blades. In practice, air is blown across a slit, along the mirrors surfaces, preventing the exhaust gases from reaching the mirrors. This causes a slight reduction of the cell length, which can be anyway accounted for. In the present measurements, it was not advisable to use such a system, as the injection of external air would have been a perturbation for the closed-cycle plant.

Each measurement step lasted about 45 min, 15 to reach a stable value of the set ammonia concentration, and 30 min available for data acquisition. We acquired two spectra per second, either in direct absorption or in second derivative. We got time series for each concentration and detection technique (e.g. Fig. 9), and took the average of each series.

The results for these averages are shown in Figs. 10 and 11, where our readings are compared with set values. Error bars are the standard deviation of these averages.

Fig. 10 shows a good agreement between direct absorption readings and set values, both with burner on (methane or diesel fuel) and with electric heating. Fig. 11 shows the same comparison with second derivative, and in this case the discrepancy when burner is off is quite large. As explained earlier about calibration of derivative technique, in order to issue mixing ratio data of the second derivative acquisitions, we first normalized the values to laser power, and then corrected the central peak height with a scale factor derived, once for ever, from the direct absorption readings (with burner on). This calibration factor is no longer valid when we change the environmental conditions, in this case the mixture composition. We can more clearly explain this point by analysing the raw acquisitions for the two techniques. Fig. 12 shows two direct absorption signals, at equal concentration, with burner on (black) and off (red), normalized with respect to laser power. The absorption with burner off (red) is clearly narrower than the black one, and its peak absorbance is higher. But this makes no difference for direct absorption, as the final result is given by the integral of the absorbance. The readings in the two cases are equal, within the experimental errors.

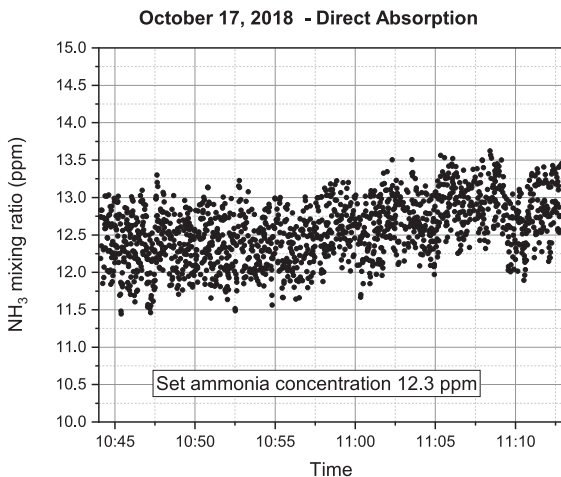


Fig. 9. Example of time series of direct absorption data.

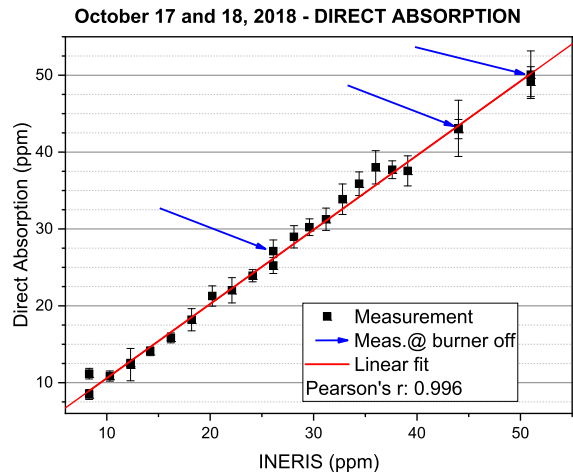


Fig. 10. Correlation of direct absorption measurements with INERIS FTIR analyser.

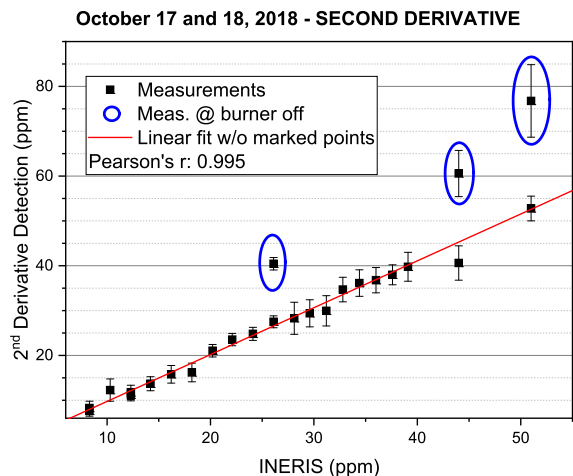


Fig. 11. Correlation of second derivative measurements with INERIS FTIR analyser.

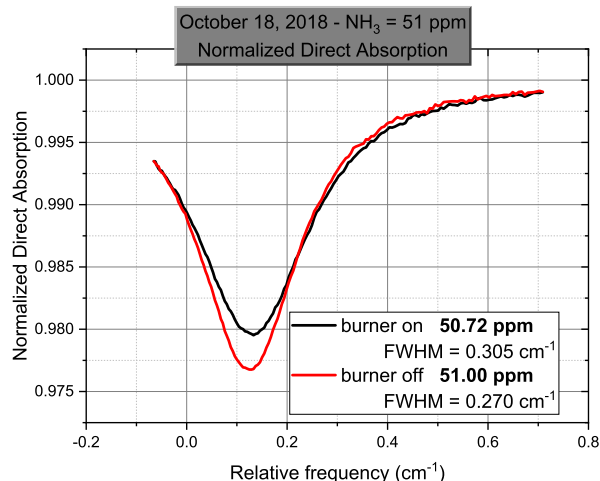


Fig. 12. Comparison of direct absorption signals in different heating conditions, normalized with respect to laser power.

The shape of the derivative signal is affected as well (Fig. 13). As in this case the information about the mixing ratio value is retrieved by peak height only, there is no simple way to account

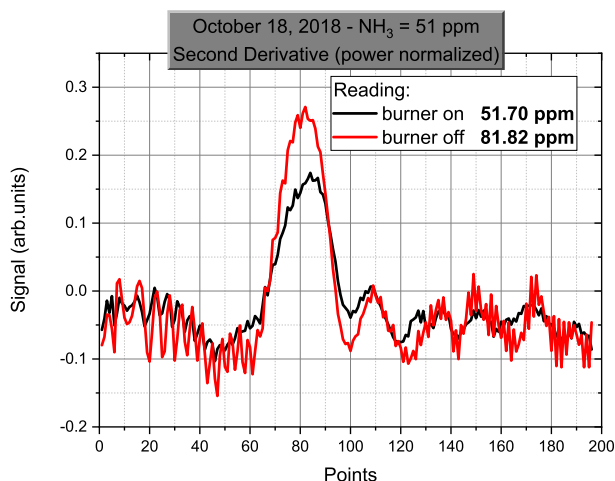


Fig. 13. Comparison of second derivative signals in different heating conditions.

for the modification of the absorption width. So the readings differ by about 50%. We can also search for correlations with the fuel. When burning, a molecule of methane (CH_4) produces two molecules of water and one of CO_2 . Diesel fuel is a mixture of hydrocarbons, and its composition is variable, in particular the ratio Hydrogen/Carbon. Table 1 shows the effects of the different fuels on gas composition. It's worth noting that with methane burner on, the increases of water and carbon dioxide, with respect to ambient air, are in a ratio very close to 2:1, as expected. On the contrary, with diesel fuel the increase of carbon dioxide is only slightly higher than that of water.

Table 2 shows how the reading of the instrument changes, in second derivative mode, with changing composition of the gas mixture. The three reported measurements are those marked with the blue frames in Fig. 11. The analyser had been calibrated with respect to the direct absorption readings. The concentration of ammonia is overestimated of about 47% in all cases. It's worth noting that this percentage doesn't vary significantly with water content. The increase of water with methane is about twice than with diesel fuel (while the increase of carbon dioxide is roughly the same), with respect to ambient air. Nevertheless this doesn't mean that a calibration with respect to the content of carbon dioxide only would be sufficient to overcome the problem. And even in this case, a simultaneous measurement of carbon dioxide should be necessary.

Table 1

Content of CO_2 and H_2O in the gas mixture in the different experimental conditions. "Amb." stays for Ambient concentration.

Burner	Day 3 Methane		Day 4 Diesel fuel	
	ON	OFF	ON	OFF
CO_2 (%)	7.77	0.05	8.7	0.09
H_2O (%)	16.01	1.53	9.0	1.78
O_2 (%)	5.16	Amb.	7.9	Amb.

Table 2

Instrument readings in second derivative mode, in the experimental conditions of Table 1. All values in ppm.

Set value	Reading @ Burner ON	Reading @ Burner OFF	Ratio OFF/ON	Fuel
26.1	27.5 ± 1.3	40.4 ± 1.4	1.47 ± 0.10	Methane
44.0	40.6 ± 3.8	60.6 ± 5.1	1.49 ± 0.30	Diesel
51.0	52.8 ± 2.8	76.7 ± 8.0	1.45 ± 0.20	Diesel

4. Conclusions and perspectives

All around the world several analytical devices exist, based on derivative techniques, which reliably measure their target molecules, also in applications when the respect of official rules must be verified. Yet, these devices usually work in quite stable environmental conditions. An example is the search for methane leaks in pipelines. In this case, the oscillations in pressure are within 5%, (absolute) temperature oscillates within 12%, water content in the air is less than 2%, CO_2 concentration is close to the ambient average. So the results of such devices are reliable enough. Also in the case of a coal thermoelectric plant, the content of carbon dioxide in the exhaust is quite stable, and the content of water vapor is 5–10% in volume. Again, optical measurements of carbon monoxide and dioxide can be easily calibrated. But, in case of a waste burner, or a remote heating plant, based on biomasses, the content of water and carbon dioxide can vary according to fuel composition and environmental conditions, both as an average [28–30], and instantaneously [31]. For instance, wooden swarf could have been stored in the open air before burning, so possibly suffering rain- or snowfall. Calibration can be a difficult or even an impossible task in these cases.

We measured ammonia, but the problem is exactly the same with any molecule, as broadening of absorption profiles occurs every time there are collisions among molecules. Project IMPRESS 2 specifically deals with biomass burning. In this case, the presence in the exhaust gases of molecules which can interfere with optical detection techniques can be very high (up to tens % in volume) and also subject to strong variations. So the alternative is either to operate the plants in controlled conditions (for instance drying the biomass before burning), or to adopt detection techniques which are intrinsically insensitive to the composition of the exhaust gases.

The present work shows that, among the optical techniques, those which are not affected by the shape of the absorptions should be preferred for this kind of measurements. They are DA, CRD and Fourier Transform InfraRed spectroscopy (FTIR), which adopts an infrared lamp as its source and can be considered a DA over a large wavelength range simultaneously. CRD is surely the most effective one, but requires very clean samples, as the mirrors must maintain their reflectivity, usually above 99.99%. For this reason, the gas must be extracted and filtered. FTIR has, with respect to DA, the advantage of measuring several molecules at time in the middle infrared, where absorptions are more intense than in the near infrared by almost two orders of magnitude. Yet, the

frequency resolution of a FTIR device is much lower than a laser-based instrument. So, changing the absorption frequency width could result in an interference among different molecular species, and a smart software is required to separate the absorption of the different molecules.

DA is the least sensitive optical technique. Yet some important improvements, with respect to the apparatus in this paper, can be easily attained. The artificial stack available at INERIS has a diameter of 15 cm, but typically the diameters of the chimneys are at least 50 cm. So, even maintaining the number of passes in the cell, longer pathlengths can easily be achieved. We selected a target wavelength in the near infrared (1512 nm), so allowing the use of optical fibers. By a proper technical design it's possible to use a mid-infrared, free propagation laser, reaching much stronger absorptions. Finally, optical fibers operating in the mid infrared region are entering the market. In the future, the same optical arrangement used for the present measurements could be used for the middle infrared, so allowing to position the laser in a safe place. This means that the need for more sensitive techniques could be less and less important, and DA could be used without renouncing to sensitivity.

Disclaimer

The content of the present paper reflects only the authors' view and EURAMET is not responsible.

CRediT authorship contribution statement

F. D'Amato: Conceptualization, Methodology, Validation, Investigation, Writing - original draft, Writing - review & editing, Visualization, Supervision, Project administration, Funding acquisition. **S. Viciani:** Conceptualization, Methodology, Software, Investigation, Formal analysis, Data curation, Validation, Writing - original draft, Visualization. **A. Montori:** Methodology, Software, Resources, Data curation, Validation. **A. Lapini:** Methodology, Software, Validation. **I. Fraboulet:** Resources, Writing - review & editing. **J. Poulleau:** Resources, Writing - review & editing.

Declaration of Competing Interest

The authors declare that they have no known competing financial interests or personal relationships that could have appeared to influence the work reported in this paper.

Acknowledgements

This project has received funding from the EMPIR programme co-financed by the Participating States and from the European Unions Horizon 2020 research and innovation programme. The authors want to thank Mr. Yannick Dupuis and Mr. Nicolas Karoski, for operating the plant during the measurement campaign. Many thanks to Mr. Massimo D'Uva for the mechanical components.

References

- [1] I.R. Burling, R.J. Yokelson, D.W.T. Griffith, T.J. Johnson, P. Veres, J.M. Roberts, C. Warneke, S.P. Urbanski, J. Reardon, D.R. Weise, W.M. Hao, J. de Gouw, Laboratory measurements of trace gas emissions from biomass burning of fuel types from the southeastern and southwestern United States, *Atmos. Chem. Phys.* 10 (2010) 11115–11130, <https://doi.org/10.5194/acp-10-11115-2010>.
- [2] K. Kohse-Höinghaus, R.S. Barlow, M. Aldén, J. Wolfrum, Combustion at the focus: laser diagnostics and control, *Proc. Combust. Inst.* 30 (2005) 89–123, <https://doi.org/10.1016/j.proci.2004.08.274>.
- [3] A. Hangauer, A. Spitznas, J. Chen, R. Strzoda, H. Link, M. Fleischer, Laser spectroscopic oxygen sensor for real time combustion optimization, *Proceedia Chem.* 1 (2009) 955–958, <https://doi.org/10.1016/j.proche.2009.07.238>.
- [4] A. Donato, D. Contini, F. Belosi, Real time measurements of PM_{2.5} concentrations and vertical turbulent fluxes using an optical detector, *Atmos. Environ.* 40 (2006) 1346–1360, <https://doi.org/10.1016/j.atmosenv.2005.10.026>.
- [5] J.A. Silver, D.S. Bomse, A.C. Stanton, Diode laser measurements of trace concentrations of ammonia in an entrained-flow coal reactor, *Sensors* 30 (1991) 1505–1511, <https://doi.org/10.1364/AO.30.001505>.
- [6] J.A. Silver, Frequency-modulation spectroscopy for trace species detection: theory and comparison among experimental methods, *Appl. Opt.* 31 (1992) 707–717, <https://doi.org/10.1364/AO.31.000707>.
- [7] P. Werle, R. Mücke, F. D'Amato, T. Lancia, Near-infrared trace-gas sensors based on room-temperature diode lasers, *Appl. Phys. B* 67 (1998) 307–315, <https://doi.org/10.1007/s003400050510>.
- [8] C.G.R. Janik, B. Carlisle, T.F. Gallagher, Two-tone frequency-modulation spectroscopy, *J. Opt. Soc. Am. B* 3 (1986) 1070–1074, <https://doi.org/10.1364/JOSAB.3.001070>.
- [9] F. D'Amato, M. De Rosa, Tunable diode lasers and two-tone frequency modulation spectroscopy applied to atmospheric gas analysis, *Opt. Las. Eng.* 37 (2002) 533–551, [https://doi.org/10.1016/S0143-8166\(01\)00089-6](https://doi.org/10.1016/S0143-8166(01)00089-6).
- [10] G.A. West, J.J. Barrett, D.R. Siebert, K. Virupaksha Reddy, Photoacoustic spectroscopy, *Rev. Sci. Instrum.* 54 (1983) 797–817, <https://doi.org/10.1063/1.1137483>.
- [11] A.A. Kosterev, L. Dong, D. Thomazy, F.K. Tittel, S. Overby, QEPAS for chemical analysis of multi-component gas mixtures, *Appl. Phys. B* 101 (2010) 649–659, <https://doi.org/10.1007/s00340-010-4183-7>.
- [12] S. Viciani, M. Siciliani de Cumis, S. Borri, P. Patimisco, A. Sampaolo, G. Scamarcio, P. De Natale, F. D'Amato, V. Spagnolo, A quartz-enhanced photoacoustic sensor for H₂S trace-gas detection at 2.6 μm, *Appl. Phys. B* 119 (2015) 21–28, <https://doi.org/10.1007/s00340-014-5991-y>.
- [13] J.J. Scherer, J.B. Paul, A. O'Keefe, R.J. Saykally, Cavity ring-down laser absorption spectroscopy: history, development, and application to pulsed molecular beams, *Chem. Rev.* 97 (1997) 25–51, <https://doi.org/10.1021/cr930048d>.
- [14] Z. Wang, Q. Wang, W. Zhang, H. Wei, Y. Li, W. Ren, Ultrasensitive photoacoustic detection in a high-finesse cavity with Pound-Drever-Hall locking, *Opt. Lett.* 44 (2019) 1924–1927, <https://doi.org/10.1364/OL.44.001924>.
- [15] F.K. Tittel, A. Sampaolo, P. Patimisco, L. Dong, A. Geras, T. Starecki, V. Spagnolo, Analysis of overtone flexural modes operation in quartz-enhanced photoacoustic spectroscopy, *Opt. Expr.* 24 (2016) 257598, <https://doi.org/10.1364/OE.24.00A682>.
- [16] B. Lee, K. Lehmann, J. Taylor, A. Yalin, A high-finesse broadband optical cavity using calcium fluoride prism retroreflectors, *Opt. Expr.* 22 (2014) 207216, <https://doi.org/10.1364/OE.22.011583>.
- [17] K. Duffin, A.J. McGettrick, W. Johnstone, G. Stewart, D.G. Moodie, Tunable diode-laser spectroscopy with wavelength modulation: a calibration-free approach to the recovery of absolute gas absorption line shapes, *J. Lightwave Technol.* 25 (2007) 3114–3125, <https://doi.org/10.1109/JLT.2007.904937>.
- [18] S.G. Razavipour, J.A. Gupta, G. Sabiston, N. Sabourin, A. Bezinger, J. Lapointe, D. Poitras, Pressure-dependent sensitivity of a single-pass methane detection system using a continuous wave distributed feedback laser at 3270 nm, *Appl. Opt.* 58 (2019) 6906–6911, <https://doi.org/10.1364/AO.58.006906>.
- [19] S. Viciani, A. Montori, A. Chiarugi, F. D'Amato, A portable quantum cascade laser spectrometer for atmospheric measurements of carbon monoxide, *Sensors* 18 (2018) 2380, <https://doi.org/10.3390/s18072380>.
- [20] D.T. Cassidy, J. Reid, Atmospheric pressure monitoring of trace gases using tunable diode lasers, *Appl. Opt.* 21 (1982) 1185–1190, <https://doi.org/10.1364/AO.21.001185>.
- [21] C.S. Goldenstein, C.L. Strand, I.A. Schultz, K. Sun, J.B. Jeffries, R.K. Hanson, Fitting of calibration-free scanned-wavelength modulation spectroscopy spectra for determination of gas properties and absorption lineshapes, *Appl. Opt.* 53 (2014) 356–367, <https://doi.org/10.1364/AO.53.000356>.
- [22] O. Bjoroey, K.H. Haugholt, T. Jaeger, Diode laser spectroscopy of gaseous HC1, *Quantum Electron.* 26 (1994) 1090–1092, <https://doi.org/10.1070/QE1996v026n12ABEH000880>.
- [23] K. Owen, E.-T. Es-sebbar, A. Farooq, Measurements of NH₃ line strengths and collisional broadening coefficients in N₂, O₂, CO₂, and H₂O near 1103.46 cm⁻¹, *J. Quant. Spectrosc. Rad. Trans.* 121 (2013) 56–68, <https://doi.org/10.1016/j.jqsrt.2013.02.001>.
- [24] A. Cifuentes, E. Marín, Implementation of a field programmable gate array-based lock-in amplifier, *Measurement* 69 (2015) 31–41, <https://doi.org/10.1016/j.measurement.2015.02.037>.
- [25] J. Wang, H. Wang, X. Liu, A portable laser photoacoustic methane sensor based on FPGA, *Sensors* 16 (2016) 1551, <https://doi.org/10.3390/s16091551>.
- [26] G.C. Giaconia, G. Greco, L. Mistretta, R. Rizzo, Exploring FPGA-based lock-in techniques for brain monitoring applications, *Electronics* 6 (2017) 18, <https://doi.org/10.3390/electronics6010018>.
- [27] M.-C. Amann, R. Hakimi, B. Borchert, S. Illek, Linewidth broadening by 1/f noise in wavelength-tunable laser diodes, *Appl. Phys. Lett.* 70 (1997) 1512–1514, <https://doi.org/10.1063/1.118603>.
- [28] J. McDonald, B. Zielinska, E.M. Fujita, J.C. Sagebiel, J.C. Chow, J.G. Watson, Fine particle and gaseous emission rates from residential wood combustion, *Environ. Sci. Technol.* 34 (2000) 2080–2091, <https://doi.org/10.1021/es9909632>.
- [29] R. Laryea-Goldsmith, J. Oakey, N.J. Simms, Gaseous emissions during concurrent combustion of biomass and non-recyclable municipal solid

- waste, Chem. Cent. J. 5 (2011) 4, <https://doi.org/10.1186/1752-153X-5-4>.
<http://journal.chemistrycentral.com/content/5/1/4>.
- [30] Y. El May, S. Dorge, M. Jeguirim, G. Trouv, R. Said, Measurement of gaseous and particulate pollutants during combustion of date palm wastes for energy recovery, Aerosol Air Qual. Res. 12 (2012) 814–825, <https://doi.org/10.4209/aaqr.2012.03.0056>.
- [31] V. Kažimírová, R. Opáth, Biomass combustion emissions, Res. Agr. Eng. 62 (Special Issue) (2016) S61–S65, <https://doi.org/10.17221/69/2015-RAE>.